

Mechanochemical Synthesis of Colloidal Silver Bromide Particles in the NaBr–AgNO₃–NaNO₃ System

F. Kh. Urakaev^{a,*}, B. B. Tatykaev^b, M. M. Burkitbayev^b, A. M. Bakhadur^b, and B. M. Uralbekov^b

^a Sobolev Institute of Geology and Mineralogy, Siberian Branch, Russian Academy of Sciences, pr. Akademika Koptyuga 3, Novosibirsk, 630090 Russia

^b Al-Farabi Kazakh National University, pr. al-Farabi 71, Almaty, 050040 Kazakhstan

*e-mail: urakaev@igm.nsc.ru

Received October 6, 2015

Abstract—X-ray diffraction and thermal analyses, electron microscopy, and dynamic light scattering have been employed to study silver bromide nanoparticles obtained by the mechanochemical exchange reaction $\text{NaBr} + \text{AgNO}_3 + z\text{NaNO}_3 = (z + 1)\text{NaNO}_3 + \text{AgBr}$ in sodium nitrate matrix (diluent and side reaction product) at $z = z_1 = 8.06$ and $z = z_2 = 4.31$. AgBr nanoparticles have been obtained in the free form by dissolving the matrix in water, and their activity in the photodegradation of methylene blue dye has been studied.

DOI: 10.1134/S1061933X16040190

INTRODUCTION

Nanoparticles of silver bromide (AgBr NPs [1–17]) and a product of its partial reduction (AgBr@Ag NPs [18–25]), nanocomposites based on them (AgBr/Ag@C, where C = Ag₃PO₄ [26–30], BiOBr [31, 32], Bi₂O₂CO₃ [33], Bi₂WO₄ [34], WO₃ [35, 36], Fe(III) [37], Fe₃O₄ [38], ZnFe₂O₄ [39], ZnO [40], K₄Nb₆O₁₇ [41], K₂Ti₄O₉ [42, 43], TiO₂ [44–47], g-C₃N₄ [48–50], modifications of carbon [51, 52], and silicates [53–55]), and hierarchical hybrid nanostructures (AgBr/Ag@C/S, where C/S = TiO₂/apatite [56], Ag₃PO₄/TiO₂ [57], Ag₃PO₄/Fe₃O₄ [58], SiO₂/Fe₃O₄ [59], SiO₂/γ-Fe₂O₃ [60], and graphene derivatives [61–63]) are promising materials to be used in different fields of science and technology.

Their catalytic properties relevant to the redox processes on interfaces (phenomena of plasmon [21, 22, 32, 63, 64] and semiconductor [21, 65–67] photocatalysis) are most in demand. They are used as catalysts for photodegradation of methylene orange [11, 19, 25, 26, 29–31, 35, 37, 38, 48, 50, 54, 57, 58], azo dyes [22, 44], methylene blue [24, 29, 33, 40, 53, 62], acid orange 7 [27, 59, 60], rhodamine B [28, 30, 32, 33, 39, 41–43, 50, 68], reactive red 120 [46], phenols [27, 52], organic contaminants [22, 63], human cancer cells [45], and bacteria and microorganisms [22, 23, 34, 44, 47, 56]. Their application for hydrogen generation [9], separation of gases [10], and CO₂ conversion into hydrocarbons [28, 51] should also be noted. In addition, they are known to possess luminescent properties [3, 61].

Almost all methods available for producing nanoparticles of AgBr and its derivatives are solution-based: ion exchange accompanied by precipitation, coprecipitation, and reduction (AgBr to Ag). Silver nitrate

and bromides of alkali metals are, as a rule, used as initial reagents. In addition, the following compounds are widely applied: cetyltrimethylammonium bromide used as a source of Br[−] ions and a surfactant [5–8, 11, 30, 45, 51]; other surfactants [4, 13]; polymers [2, 10, 23], including polyols [1, 18, 24] and polyelectrolytes [11, 20]; and products obtained from tissues of animals [4, 16] and plants [20]. “Nanoreactors” are frequently used for realization of the solution-based methods. Aqueous–organic microemulsions [7, 8, 48]; membranes [10]; and meso- and nanoporous natural silicates [53–55, 68], e.g., attapulgite [68], should be noted as such systems. Moreover, the synthesis processes are activated by heating under pressure (hydro- and solvothermal methods [22, 40, 49, 60]), electrochemical methods [4, 61], and ultrasonic [1, 12, 20, 52, 57] or microwave [20, 41, 42] radiation. Occasionally, AgBr NPs are produced by reactions in suspensions [16, 17], the sol–gel method [47], crystal growing [3], from films [14, 19], and via the solid-phase synthesis [9, 25].

The AgBr NPs synthesized in the majority of the cited works had spherical [6, 16, 17, 25, 30, 60] or cubic [11, 15, 25, 29] shapes. However, such nanoparticles and composite structures based on them may also be produced as porous spheres [1, 16], plates [11, 18, 36], tubes [19], wires [11, 19], rods [6, 40, 57], and magnetic particles [38, 39, 58–60].

As applied to the subject of this article, it should be noted that, in contrast to silver chloride and iodide nanoparticles, AgBr NPs have not been produced by mechanochemical methods. Mechanochemical synthesis of AgCl and AgI NPs has been described in detail in [69, 70]. In particular, it has been shown that they may be obtained by attrition in a mortar [69] and

mechanical activation (MA) in ordinary [69] and planetary-type [70] mills.

As in [69, 70], the dilution method was used in this work for mechanochemical synthesis of AgBr NPs via reaction $\text{NaBr} + \text{AgNO}_3 + z\text{NaNO}_3 = (z + 1)\text{NaNO}_3 + \text{AgBr}$, while the values of dilution parameter z were calculated by the following formulas [71]:

$$z_1 = \rho_3[\rho_2 M_1 - 0.0937\rho_1 M_2]/0.0937\rho_1\rho_2 M_3 = 8.06, \quad (1)$$

$$z_2 = 2.28\rho_3(\rho_2 M_1 + \rho_1 M_2)/\rho_1\rho_2 M_3 = 4.31, \quad (2)$$

where M_i and ρ_i are the molecular masses and densities of the reagents ($i = 1$, NaBr, $M_1 = 102.89$, $\rho_1 = 3.21$ g/cm³; $i = 2$, AgNO₃, 169.87, 4.35) and the diluent ($i = 3$, NaNO₃, 84.99, 2.26). Formulas (1) and (2) were derived based on the trimodal particle size distribution and the hardness values of the reagents and the diluent: the harder particles “cut” the softer ones, thereby transferring them into the octahedral and tetrahedral cavities. When the diluent material is hardest, the z value obtained by Eq. (1) must be used. When the diluent material is softest, the z obtained by Eq. (2) may be applied. Unfortunately, we had not found AgNO₃ hardness in the literature; therefore, the experiments were carried out at both $z = z_1$ and $z = z_2$.

EXPERIMENTAL

MA was performed in a 2SL steel two-cylinder water-cooled planetary-type mill (Russia) with a cylinder volume of 250 cm³. Balls with a diameter of 0.673 cm and a weight of 1.245 g were used. Experiments were carried out at $z = z_1$ and $z = z_2$ in cylinders 1 and 2, respectively. The weight (number) of the balls and the weighed portions of the charge in the cylinders after their balancing were as follows: for no. 1, 280.15 g (225) and 10.013 g; for no. 2, 277.49 g (223) and 8.024 g. The ratios between the weights of balls and samples were $280.15/10.013 \approx 28$ and $277.49/8.024 \approx 35$ for cylinders 1 and 2, respectively.

The MA regime was as follows. MA was performed for 7 min at a cage rotation rate of 210 and for 7 min at 280 rpm; then, the cylinders were opened and recharged. After that, MA was carried out for 7 min at 350 rpm and 7 min at 420 rpm; then, samples were taken. The total MA duration was 28 min.

The X-ray diffraction (XRD) analysis was performed with a D8 ADVANCE diffractometer (Bruker AXS) using monochromatic radiation of copper at a scanning step of $2\theta = 0.02^\circ$ and a data accumulation time at one point of 1 s. The angular positions and intensities of reflections, as well as the phase compositions of the samples were determined by processing the XRD data using the EVA.exe, RIR (Reference Intensity Ratio), and PCPDFWIN software, as well as the PGF-2 database (see also [69, 70]).

Thermal analyses (thermogravimetry (TG) and differential scanning calorimetry (DSC)) were carried out under nitrogen with a NETZSCH 449F3A-

0372 M instrument at temperatures up to 1000°C and a heating rate of 10 K/min.

The morphological features and sizes of nanoparticles were determined using a JEM-1011 transmission electron microscope (TEM) (JEOL, Japan) equipped with a Morada digital camera (OLYMPUS). Samples (10 mg) were placed into ampules with hexane (3 mL), and one droplet of the resulting suspension was applied onto standard collodion-coated copper grids. TEM images were obtained with a resolution up to 5 nm at an accelerating voltage of 100 kV.

The size distribution of AgBr nanoparticles was determined by dynamic light scattering (DLS) with a Zetasizer Nano ZS90 instrument (Malvern, United Kingdom). Powdered samples removed from the cylinders after MA had been completed were studied. Fairly well reproducible results were obtained when 1 mg of a powder was dispersed in 10 mL of water.

AgBr nanoparticles were separated from the diluent (NaNO₃) matrix by washing with water as follows: samples (≈ 500 mg) were dissolved in water (10 mL) in glass centrifuge tubes. Powders resulting from triple decanting were dried at 85°C.

The kinetics of methylene blue photodegradation in the presence of the obtained powders was studied spectrophotometrically by measuring the optical density of dye solutions at a wavelength of 665 nm as a function of the time of their irradiation by sunlight.

RESULTS AND DISCUSSION

Let us consider the properties and characteristics of the products resulting from the mechanochemical synthesis.

X-ray Diffraction Analysis

The results of the XRD analysis of MA products are presented in Fig. 1. It can be seen that reactions (1) and (2) have been completed, because only the lines attributed to the desired product (AgBr) and diluent (NaNO₃) are present. The processing of the diffraction patterns has yielded the following data: at $z = z_1$ (Fig. 1a), the sample contains NaNO₃ (82.1%) and AgBr (17.9%), with the crystal size being $L = 70$ nm; at $z = z_2$ (Fig. 1b), NaNO₃ (73.0%), AgBr (27.0%), and $L = 73$ nm. The intensity ratio between the maximum reflection lines for NaNO₃ and AgBr in Figs. 1a and 1b is close to the z_1/z_2 ratio, as in [70].

Thermal Analysis

In addition to the XRD data, Fig. 2 shows the TG/DSC curves for samples resulting from the MA reaction. The analysis of the DSC curves demonstrates that the samples exhibit the thermal effects of the same two substances. AgBr is characterized by a phase transition at $\approx 260^\circ\text{C}$ and a melting temperature of $\approx 425^\circ\text{C}$, while NaNO₃ has a melting temperature of

$\approx 305^\circ\text{C}$. According to the TG data, a noticeable mass loss begins to be observed above 500°C due to the decomposition of NaNO_3 and evaporation of AgBr , while, at 1000°C , it reaches 72.12% at $z = z_1$ (Fig. 2a) and 57.75% at $z = z_2$ (Fig. 2b).

Let us perform some calculations. At $z = z_1$, the decomposition of NaNO_3 to Na_2O and the complete evaporation of AgBr would result in a mass losses of 58.62 and 19.61%, respectively, while, at $z = z_2$, they would be 51.50 and 29.38%, respectively. On the whole, they come to 78.23% ($z = z_1$) and 80.88% ($z = z_2$). In the first and second cases, the differences between the calculated and experimental values are $78.23\% - 72.12\% = 6.11\%$ and $80.88\% - 57.75\% = 23.13\%$, respectively. It is clear that sodium oxide completely remains preserved in the crucibles because of its high thermal stability. Hence, by analogy with AgCl [70], we may believe, that the excess mass loss of the samples resulting from the MA reaction is due to the evaporation of silver bromide alone: $72.12\% - 58.62\% = 13.5\%$ (Fig. 2a) and $57.75\% - 51.50\% = 6.25\%$ (Fig. 2b). The inflections in the TG curves also confirm the existence of two mechanisms responsible for the mass loss of the synthesized samples.

Transmission Electron Microscopy

TEM micrographs of the samples resulting from the MA reaction are shown in Fig. 3. In the sample synthesized at $z = z_1$, the sizes of the majority of AgBr nanoparticles lie in a range of 10–90 nm; however, larger particles (up to 200 nm) are also present. The nanoparticle size distribution of the sample synthesized at $z = z_2$ is narrower and corresponds to a range of 30–80 nm (see the fragment of the micrograph in the insert to Fig. 3). At the same time, it can be seen that the nanoparticles are almost spherical.

Dynamic Light Scattering

Figure 4 presents AgBr nanoparticle size distribution histograms obtained from the DLS data. These histograms show the dynamics of variations in the distribution of the particles in their aqueous dispersion. At $z = z_2$, the average particle size at the initial moment of measurements was 92 nm (Fig. 4a), while, already in ≈ 2 min, it appeared to be 119 nm (Fig. 4b). At the higher nanoparticle concentration ($z = z_2$), the average particle size was 168 nm already at the initial moment of the measurements (Fig. 4c). Note that, in order to prevent nanoparticles from fast coagulation, the measurements were carried out in highly diluted systems, i.e., near the limit of the instrument sensitivity; therefore, nanoparticles with very small or large sizes remained, possibly, unrecorded, if their contents were low.

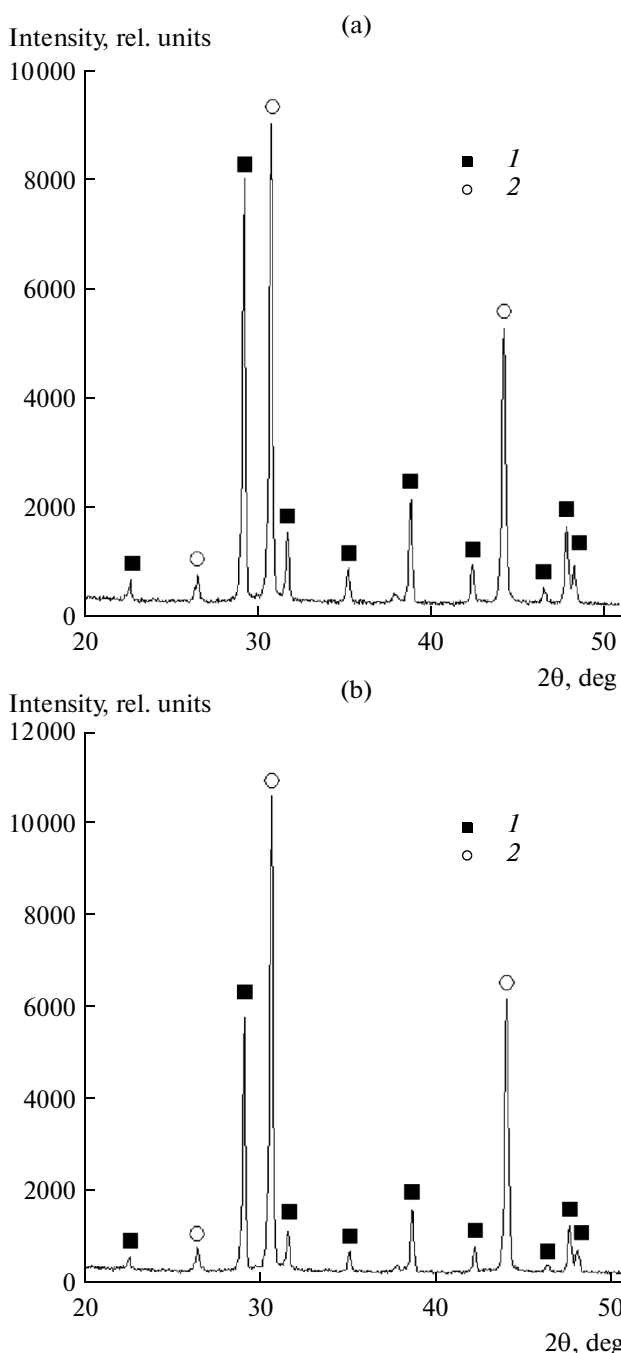


Fig. 1. Results of XRD analysis of samples resulting from MA performed in a range of $2\theta = 20^\circ - 50^\circ$: $z_1 =$ (a) $z_1 = 8.06$ and (b) $z_2 = 4.31$. Reflection assignment: (1) NaNO_3 (PDF 79-2056) and (2) AgBr (PDF 79-149).

Isolation of Free Nanoparticles

Figure 5a shows the XRD data on the sample resulting from washing a product of the MA reaction performed at $z = z_2$. Only the AgBr phase can be seen with crystallite size $L = 63$ nm (compare with the data for reference AgBr in Fig. 5b). Nearly the same size

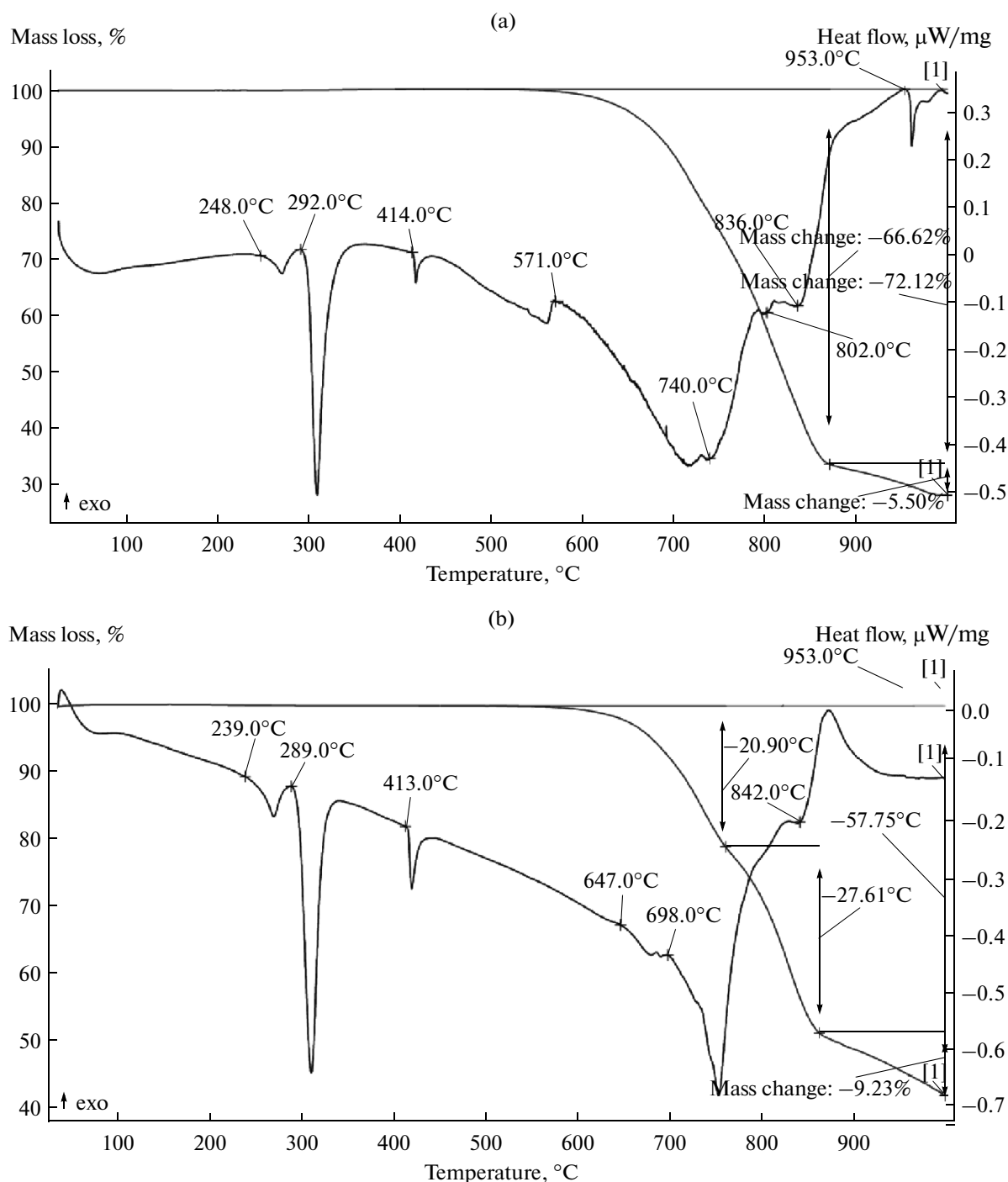


Fig. 2. Results of thermal analysis for samples obtained by MA at $z =$ (a) z_1 and (b) z_2 .

$L = 60$ nm has been obtained by processing the XRD data on the sample synthesized at $z = z_1$.

It may be stated that the sizes of the coherent-scattering regions for free AgBr particles are comparable with those for particles in the diluent matrix (Fig. 1) and with the particle sizes in TEM micrographs (Fig. 3), as well as those obtained by DLS (Fig. 4a).

When storing and studying the obtained samples, we made efforts to prevent them from the action of visible light. However, according to the published data, the photocatalytic activity of AgBr@Ag NPs is higher than that of AgBr NPs. Therefore, AgBr NPs were further washed without protection from sunlight. The TEM micrograph of such AgBr NPs synthesized at $z = z_1$ is shown in Fig. 6. It can be seen that nanoparticles

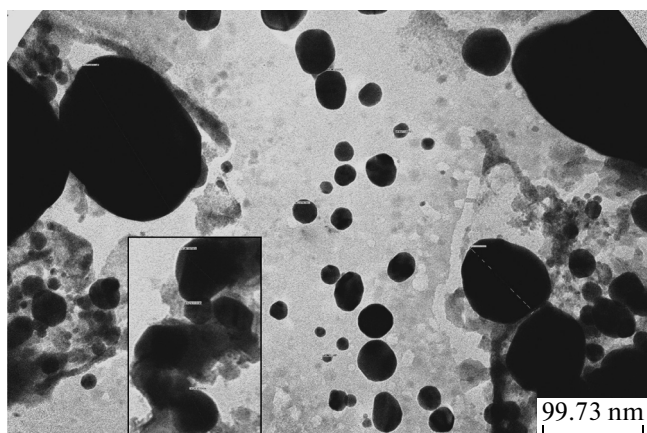


Fig. 3. TEM image ($\times 300000$) of a sample obtained by MA at $z = z_1$. A fragment of a micrograph taken under similar conditions from a sample synthesized at $z = z_2$ is shown in the inset.

of the product of silver bromide photolysis (silver metal) with sizes from a few to 30 nm are present on the surface of rather large AgBr particles (~ 100 nm). Moreover, very small individual AgBr and Ag nanoparticles are also observed on the substrate. We have found no similar micrographs of AgBr@Ag NPs in the literature. Very close results and their interpretation have been reported in [22, 32, 48, 72–74].

Photocatalytic Properties of Nanoparticles

As has been noted in the Introduction, AgBr NPs and nanostructures based on them are predominantly demanded for the photocatalytic decomposition of harmful substances. Figure 7 (curve 4) illustrates the data on the decoloration of an aqueous 10 mg/L methylene blue solution (100 mL) under the action of sunlight in the presence of AgBr@Ag composite nanoparticles (250 mg) obtained in the way described in the previous section. It is obvious that they possess a high photocatalytic activity (the dye is completely decomposed over 6 h). It should be emphasized that, being exposed to sunlight in the absence of AgBr@Ag nanoparticles, the dye is decomposed by only $\sim 30\%$ over the same time (curve 1).

Silver bromide obtained from a NaBr solution by adding an equimolar amount of AgNO₃ was used for comparison. The dried precipitate was exposed to sunlight for 7 h, while being periodically attrited in an agate mortar. Then, it was introduced into methylene blue solutions. Note that its photocatalytic activity (Fig. 7, curve 3) is slightly lower than that of AgBr@Ag nanocomposite (curve 4).

CONCLUSIONS

The production methods and properties of AgBr nanoparticles and composites based on them have

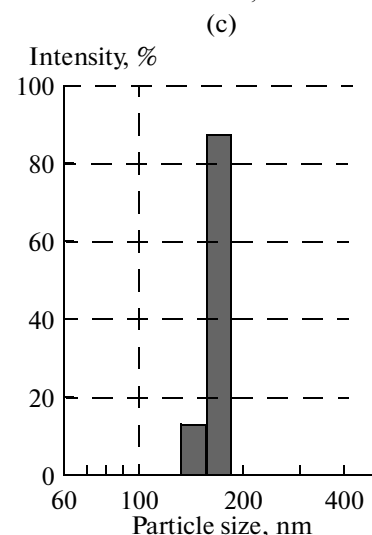
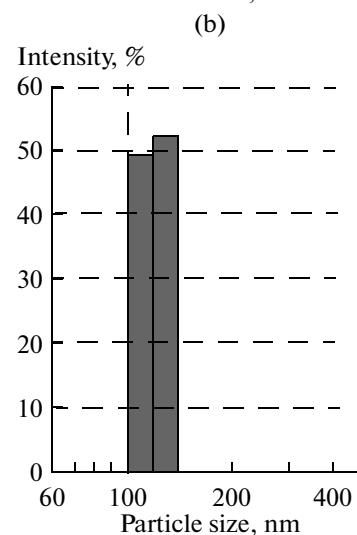
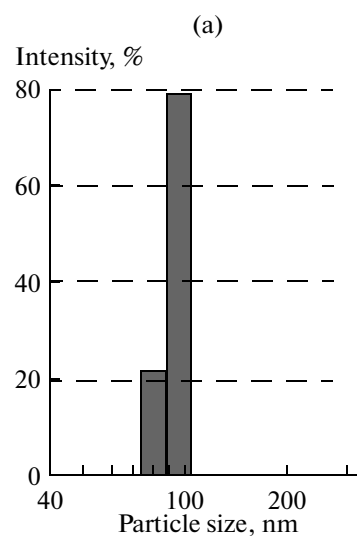


Fig. 4. AgBr nanoparticle size distribution histograms plotted from the DLS data: (a) $z = z_1$, initial measurement, (b) measurement carried out in 106 s, and (c) $z = z_2$, initial measurement.

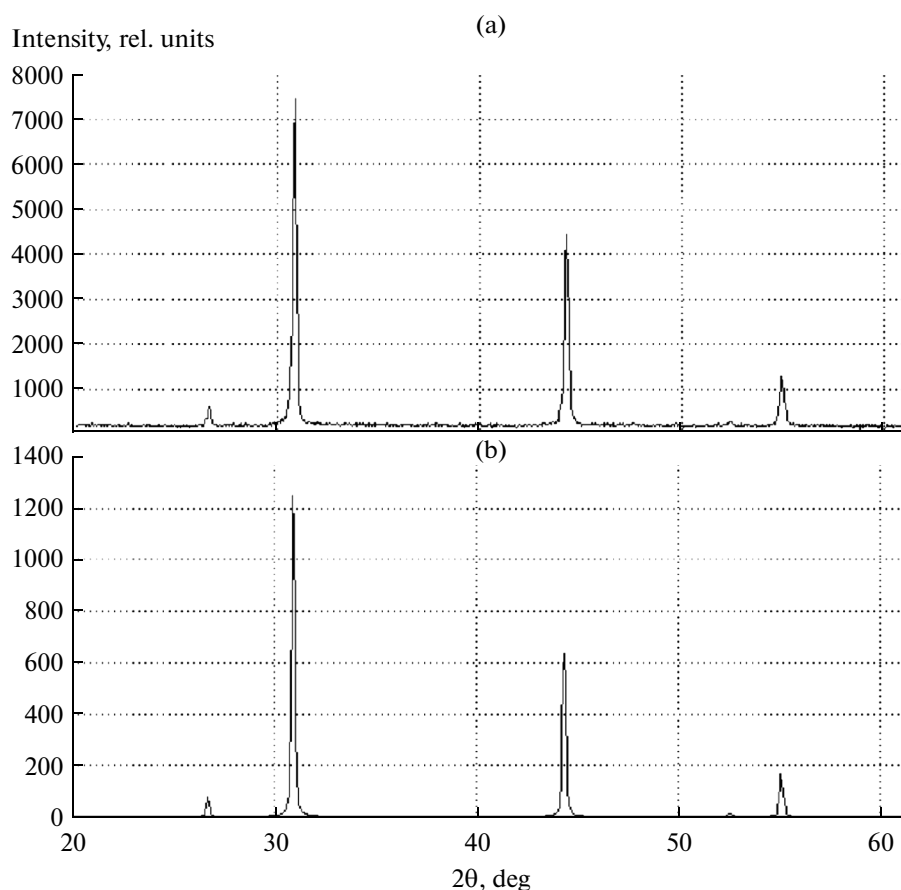


Fig. 5. Diffraction patterns measured for different silver bromide samples: (a) after washing with water a sample obtained by MA at $z = z_2$ and (b) reference AgBr sample (PDF 79-149).

been briefly reviewed. It has, for the first time, been proposed to synthesize AgBr nanoparticles by the mechanochemical method with the use of a diluent.

Silver bromide nanoparticles have been synthesized via the $\text{NaBr} + \text{AgNO}_3 + z\text{NaNO}_3 = (z + 1)\text{NaNO}_3 + \text{AgBr}$ reaction in a diluent (NaNO_3) matrix at two theoretically calculated values of dilution parameter $z = z_1 = 8.06$ and $z = z_2 = 4.31$ by mechanical activation of mixed salts in a water-cooled steel planetary-type ball mill.

X-ray diffraction and thermal analysis have been used to prove that the reaction proceeds completely and to determine the sample phase composition. Coherent-scattering region sizes $L(z_1) = 70$ nm and $L(z_2) = 73$ nm have been calculated for AgBr nanoparticles. As whole, the results obtained agree with the data obtained for the studied samples by electron microscopy and dynamic light scattering.

Synthesized silver bromide nanoparticles have been isolated in the free form by washing out the matrix with water, and their photocatalytic activity with respect to methylene blue has been studied.

ACKNOWLEDGMENTS

We are grateful to V.I. Antonyuk, E.E. Dil'mukhambetov, Zhanar Nurakhmetova, and

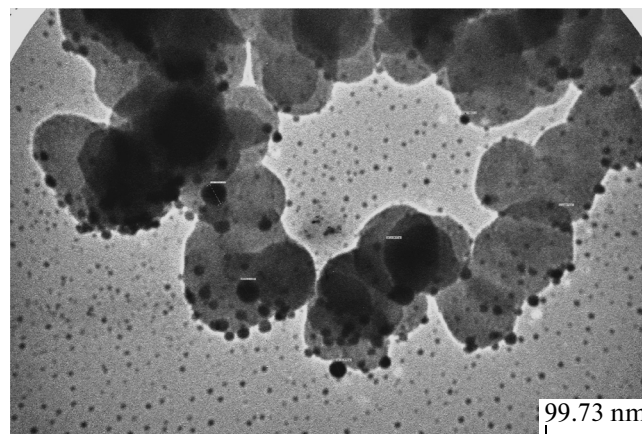


Fig. 6. TEM micrograph ($\times 300000$) taken from a sample obtained by MA at $z = z_1$ and washed with water.

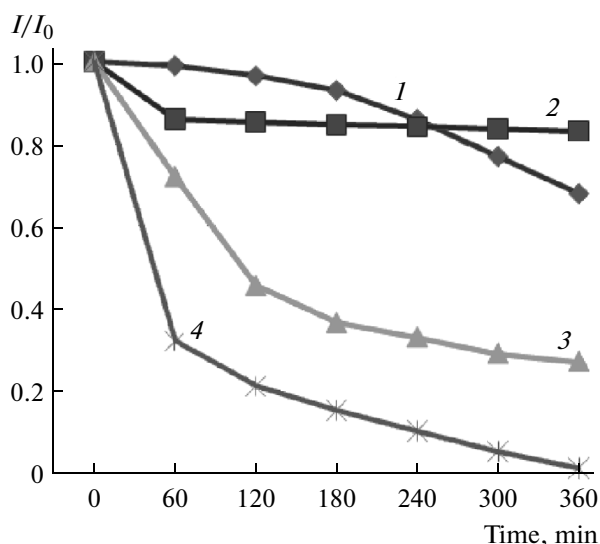


Fig. 7. Reduced optical densities I/I_0 of methylene blue solution as depending on time t of irradiation by sunlight (1) in the absence of a catalyst, (2) in the presence of AgBr@Ag composite nanoparticles but in the dark, (3) in the presence of reference silver bromide obtained by precipitation, and (4) in the presence of AgBr@Ag nanoparticles.

Zhandos Ukibaev for their help in the analytical experiments.

This work was supported by “Program-Purpose Financing of the Republic of Kazakhstan” (contract no. 586 of April 7, 2015) and the Russian Foundation for Basic Research (project no. 15-05-03980a).

REFERENCES

- Abbasi, A.R. and Morsali, A., *Ultrason. Sonochem.*, 2012, vol. 19, p. 540.
- Anderson, R., Buscall, R., Eldridge, R., et al., *Colloids Surf. A*, 2014, vol. 459, p. 58.
- Baranov, P.G., Romanov, N.G., Khramtsov, V.A., and Vikhnin, V.S., *Nanotechnology*, 2001, vol. 12, p. 540.
- Bartlett, T.R., Sokolov, S.V., and Compton, R.G., *ChemistryOpen*, 2015, vol. 4, p. 600.
- Chakraborty, M., Hsiao, F.-W., Naskar, B., et al., *Langmuir*, 2012, vol. 28, p. 7282.
- Gupta, V.K.N., Mehra, A., and Thakkar, R., *Colloids Surf. A*, 2012, vol. 393, p. 73.
- Husein, M.M., Rodil, E., and Vera, J.H., *J. Nanopart. Res.*, 2007, vol. 9, p. 787.
- Husein, M.M., Rodil, E., and Vera, J.H., *Langmuir*, 2006, vol. 22, p. 2264.
- Kobayashi, B., Yamamoto, R., Ohkita, H., et al., *Top. Catal.*, 2013, vol. 56, p. 618.
- Koh, J.H., Kang, S.W., Park, J.T., et al., *J. Membr. Sci.*, 2009, vol. 339, p. 49.
- Lee, Y.S., Lee, H.-J., and Choi, W.S., *Langmuir*, 2014, vol. 30, p. 9584.
- Moosavi, R., Abbasi, A.R., Yousefi, M., et al., *Ultrason. Sonochem.*, 2012, vol. 19, p. 1221.
- Ray, M. and Paria, S., *Ind. Eng. Chem. Res.*, 2011, vol. 50, p. 11601.
- Seki, K., Yanagi, H., Kobayashi, Y., et al., *Phys. Rev. B: Condens. Matter*, 1994, vol. 49, p. 2760.
- Shiba, F. and Okawa, Y., *J. Phys. Chem. B*, 2005, vol. 109, p. 21664.
- Yang, M., Zhao, J.-G., and Li, J.-J., *Colloids Surf. A*, 2007, vol. 295, p. 81.
- Yang, M. and Zhou, K., *Appl. Surf. Sci.*, 2011, vol. 257, p. 2503.
- An, C., Wang, J., Jiang, W., et al., *Nanoscale*, 2012, vol. 4, p. 5646.
- Choi, W.S. Byun, G.Y., et al., *ACS Appl. Mater. Interfaces*, 2013, vol. 5, p. 11225.
- Dong, Y.-Y., He, J., Sun, S.-L., et al., *Carbohydr. Res.*, 2013, vol. 98, p. 168.
- Jiang, J., Li, H., and Zhang, L., *Chem.-Eur. J.*, 2012, vol. 18, p. 6360.
- Kuai, L., Geng, B., Chen, X., et al., *Langmuir*, 2010, vol. 26, p. 18723.
- Suchomel, P., Kvitek, L., Panacek, A., et al., *PLoS ONE*, 2015, vol. 10, p. 0119202.
- Wang, Z., Liu, J., and Chen, W., *Dalton Trans.*, 2012, vol. 41, p. 4866.
- Zhu, M., Chen, C., Chen, P., et al., *Phys. Chem. Chem. Phys.*, 2013, vol. 15, p. 12709.
- Cao, J., Luo, B., Lin, H., et al., *J. Hazard. Mater.*, 2012, vols. 217–218, p. 107.
- Katsumata, H., Hayashi, T., Taniguchi, M., et al., *Mater. Sci. Semicond. Process.*, 2014, vol. 25, p. 68.
- Wang, B., Gu, X., Zhao, Y., and Qiang, Y., *Appl. Surf. Sci.*, 2013, vol. 283, p. 396.
- Wang, W.S., Du, H., Wang, R.X., et al., *Nanoscale*, 2013, vol. 5, p. 3315.
- Wang, X., Yuan, S., Chen, S., et al., *Res. Chem. Intermediates*, 2015, vol. 41, p. 5137.
- Lin, H.L., Cao, J., Luo, B.D., et al., *Chin. Sci. Bull.*, 2012, vol. 57, p. 2901.
- Ye, L., Liu, J., Gong, C., et al., *ACS Catal.*, 2012, vol. 2, p. 1677.
- Jin, L., Zhu, G., Hojamberdiev, M., et al., *Ind. Eng. Chem. Res.*, 2014, vol. 53, p. 13718.
- Zhang, L.S., Wong, K.H., Yip, H.Y., et al., *Environ. Sci. Technol.*, 2010, vol. 44, p. 1392.
- Cao, J., Luo, B., Lin, H., and Chen, S., *J. Hazard. Mater.*, 2011, vol. 190, p. 700.
- Wang, P., Huang, B., Qin, X., et al., *Inorg. Chem.*, 2009, vol. 48, p. 10697.
- Yu, H., Xu, L., Wang, P., et al., *Appl. Catal. B*, 2014, vol. 144, p. 75.
- Cao, Y., Li, C., Li, J., et al., *Nanoscale Res. Lett.*, 2015, vol. 10, p. 251.
- Li, X., Tang, D., Tang, F., et al., *Mater. Res. Bull.*, 2014, vol. 56, p. 125.
- Pirhashemi, M. and Habibi-Yangjeh, A., *Appl. Surf. Sci.*, 2013, vol. 283, p. 1080.

41. Cui, W., Wang, H., Liang, Y., et al., *Chem. Eng. J.*, 2013, vol. 230, p. 10.
42. Liang, Y., Lin, S., Liu, L., et al., *Mater. Res. Bull.*, 2014, vol. 56, p. 25.
43. Liang, Y., Lin, S., Liu, L., et al., *Chin. J. Inorg. Chem.*, 2014, vol. 30, p. 2675.
44. Hu, C., Lan, Y., Qu, J., et al., *J. Phys. Chem. B*, 2006, vol. 110, p. 4066.
45. Seo, J.H., Jeon, W.I., Dembereldorj, U., et al., *J. Hazard. Mater.*, 2011, vol. 198, p. 347.
46. Velmurugan, R., Sreedhar, B., and Swaminathan, M., *Chem. Cent. J.*, 2011, vol. 5, p. 46.
47. Wang, X. and Lim, T.T., *Water Res.*, 2013, vol. 47, p. 4148.
48. Li, Y., Zhao, Y., Fang, L., et al., *Mater. Lett.*, 2014, vol. 126, p. 5.
49. Xu, Y., Xu, H., Yan, J., et al., *Colloids Surf. A*, 2013, vol. 436, p. 474.
50. Yang, Y., Guo, W., Guo, Y., et al., *J. Hazard. Mater.*, 2014, vol. 271, p. 150.
51. Fang, Z., Li, S., Gong, Y., et al., *J. Saudi Chem. Soc.*, 2014, vol. 18, p. 299.
52. Shi, H., Chen, J., Li, G., et al., *ACS Appl. Mater. Interfaces*, 2013, vol. 5, p. 6959.
53. Pourahmad, A., Sohrabnezhad, Sh., and Kashefian, E., *Spectrochim. Acta A*, 2010, vol. 77, p. 1108.
54. Zhang, J., Li, B., and Yang, W., *Micropor. Mesopor. Mater.*, 2014, vol. 194, p. 66.
55. Zang, Y., Farnood, R., and Currie, J., *Chem. Eng. Sci.*, 2009, vol. 64, p. 2881.
56. Elahifard, M.R., Rahimnejad, S., Haghghi, S., and Gholami, M.R., *J. Am. Chem. Soc.*, 2007, vol. 129, p. 9552.
57. Xi, M., Li, J., Wu, L., and Li, X., *ECS J. Solid State Sci. Technol.*, 2015, vol. 4, no. 8, p. Q67.
58. Wang, Z., Yin, L., Chen, Z., et al., *J. Nanomater.*, 2014, vol. 2014, p. 150150.
59. Li, G., Wong, K.H., Zhang, X., et al., *Chemosphere*, 2009, vol. 76, p. 1185.
60. Tian, B., Wang, T., Dong, R., et al., *Appl. Catal. B*, 2014, vol. 147, p. 22.
61. Jiang, D., Du, X., Liu, Q., et al., *Chem. Commun.*, 2015, vol. 51, p. 4451.
62. Shah, M.S.A.S., Kim, W.-J., Park, J., et al., *ACS Appl. Mater. Interfaces*, 2014, vol. 6, p. 20819.
63. Zhu, M., Chen, P., and Liu, M., *ACS Nano*, 2011, vol. 5, p. 4529.
64. Zhang, X., Chen, Y.L., Liu, R.S., and Tsai, D.P., *Rep. Prog. Phys.*, 2013, vol. 76, p. 046401.
65. Hoffmann, M.R., Martin, S.T., Choi, W., and Bahnemann, D.W., *Chem. Rev.*, 1995, vol. 95, p. 69.
66. Kisch, H., *Angew. Chem., Int. Ed. Engl.*, 2013, vol. 52, p. 812.
67. Wang, H., Zhang, L., Chen, Z., et al., *Chem. Soc. Rev.*, 2014, vol. 43, p. 5234.
68. Yang, Y. and Zhang, G., *Appl. Clay Sci.*, 2012, vols. 67–68, p. 11.
69. Tatykaev, B.B., Burkitbayev, M.M., Uralbekov, B.M., and Urakaev, F.Kh., *Acta Phys. Pol. A*, 2014, vol. 126, p. 1044.
70. Urakaev, F.Kh., Burkitbaev, M.M., Tatykaev, B.B., and Uralbekov, B.M., *Colloid J.*, 2015, vol. 77, p. 641.
71. Urakaev, F.Kh., *Mendeleev Commun.*, 2011, vol. 21, p. 266.
72. Lin, S., Hu, J., Liu, L., et al., *Chem. Bull. / Huaxue Tongbao*, 2014, vol. 77, p. 37.
73. Botasin, S. and Mendez, E., *J. Nanopart. Res.*, 2013, vol. 15, p. 1526.
74. Liang, Y., Lin, S., Liu, L., et al., *Appl. Catal. B*, 2015, vol. 164, p. 192.

Translated by A. Kirilin